COMMUN. MATH. SCI.
Vol. 17, No. 1, pp. 175–192

DYNAMIC BIFURCATION AND TRANSITION IN THE RAYLEIGH-BÉNARD CONVECTION WITH INTERNAL HEATING AND VARYING GRAVITY*

DAOZHI HAN†, MARCO HERNANDEZ‡, AND QUAN WANG§

Abstract. In this article, we study the dynamic transition of the Rayleigh-Bénard convection with internal heating and varying gravity. We show that this problem can only undergo a continuous or catastrophic transition, and the specific type is completely determined by the sign of a parameter – referred to as the transition number – that depends on the aspect ratio. Through numerical simulations we compute, for six qualitatively different heating sources, the corresponding value of the transition number, and find that the transition is always continuous. In particular, after transition, the system bifurcates from a basic steady state to a family of stable steady states, homeomorphic to $\mathbb{S}^1$, that describe the heating convection. Furthermore, upon varying the aspect ratio immediately after the first transition has occurred, we find the existence of a second transition, which is always catastrophic. More precisely, there exists a family of discrete values of the aspect ratio, which are the discontinuity points of the transition number, at which the transition is catastrophic and the number of convection rolls changes.

Keywords. Rayleigh-Bénard convection; internal heating sources; dynamic transition; continuous and catastrophic transition; reduced equation.

AMS subject classifications. 76D10; 76E06; 76E20; 37L15; 37L99.

1. Introduction

The Rayleigh-Bénard convection is a type of natural convection, namely, a thermally convected fluid flow whose dynamics are due to a non-uniform temperature distribution on a flat horizontal fluid layer heated from below. Such flows develop as a result of convective instability when the static vertical temperature gradient, i.e. the gradient that would be present in a motionless fluid under the same conditions, is sufficiently large.

The importance of convection phenomena cannot be overestimated. Problems pertaining to the Rayleigh-Bénard convection have been of great interest for some time in fields ranging from numerical analysis to experimental physics, and even in the geophysical sciences and many engineering applications [1–4].

For the Rayleigh-Bénard problem, the principle of exchange of stabilities – referred to here as the PES condition, see Section 4 for a detailed discussion – was first addressed by Pellew and Southwell [5]. They considered the case of a fluid in the Boussinesq approximation with uniform heating from below, where the equations governing instability have special symmetries that make all the eigenvalues of the linearized problem real-valued. The bifurcation associated with the Rayleigh-Bénard convection at the onset of instability is well-known, see e.g. [2, 6] for the linear stability analysis, and [7, 8] for nonlinear theories, among many others. Recently, Ma and Wang [7, 9] have shown that the Rayleigh-Bénard problem bifurcates from the basic steady state to an attractor containing exactly eight singular points when the Rayleigh number crosses the first critical

*Received: February 10, 2018; Accepted (in revised form): November 3, 2018. Communicated by Jie Shen.

†Department of Mathematics and Statistics, Missouri University of Science and Technology, Rolla, MO 65409, USA (handaoz@mst.edu).

‡Department of Mathematics, Indiana University, Bloomington, IN 47405, USA (hernmarc@indiana.edu).

§Department of mathematics, Sichuan University, Chengdu, China (wqxihujunzi@126.com).

Rayleigh number, under physically sound boundary conditions. Hsia [10] studied the dynamic transitions of the Rayleigh-Bénard problem with rotation. Further results in this direction can be found in [11, 12].

In 1987, Pradhan and Samal [13] pointed out that in large scale atmospheric convection phenomena the effect of variable gravity can be important and should not be neglected. Thus in a real atmospheric convection scenario, variable gravity effects and internal heating sources should be considered. Straughan [14] studied the case of a variable gravity field, where his results indicate that decreasing or increasing the relative intensity of the gravitational force can accelerate or delay the occurrence of convection. In the context of arbitrary heat sources and varying gravity, Herron [15,16] showed that the PES condition holds as long as the product of the gravity field and the integral of the heat sources is nonnegative throughout the layer. In order to have a complete understanding of the heat circulation of the atmosphere it is thus crucial to study the dynamic transitions of the Rayleigh-Bénard convection with internal heating and varying gravity.

Our first goal is to use the dynamic transition theory developed by Ma and Wang [17] to tackle this problem. The main philosophy of this theory is to search for the full set of transition states, giving a complete characterization of stability and transition of the bifurcated solutions at the onset of instability. The set of transition states is often represented by a local attractor. Following this philosophy, the dynamic transition theory aims to identify the transition states and to classify them both dynamically and physically. One important ingredient of the theory is the introduction of a new classification scheme for transitions into three types: continuous, catastrophic, and random. Roughly speaking, a continuous transition means that the basic steady state bifurcates to a local attractor; a catastrophic transition means that a system will jump to another state, and a random transition indicates that both continuous and catastrophic transitions are possible depending on the initial perturbation. In this work we show that the type of transition of the Rayleigh-Bénard convection with internal heating and varying gravity can be uniquely determined by the sign of a parameter, called transition number, whose value can be efficiently computed numerically.

Details of the topological structure of the flow patterns, such as the number of roll patterns, depend crucially on the aspect ratio; however, previous studies did not pay any attention to the relationship between the aspect ratio and the topological structure of the bifurcated solutions. Thus, our second aim is to perform a more detailed analysis of this issue, and to determine, for instance, at which values of the aspect ratio the roll pattern changes its topological structure.

The core of our analysis pertains to the task of obtaining a set of reduced ordinary differential equations from the original system of partial differential equations. This reduced system corresponds to the the full system restricted to its center-unstable manifold. The dynamic transition is then studied using the reduced system following the ideas from the dynamic transition theory, e.g. the transition number is derived from the reduced equations through simple algebraic manipulations.

The paper is organized as follows. In Section 2 we introduce the governing equations and the basic steady states whose stability we intend to study. The stream-function and abstract Hilbert space formulations of the problem are briefly discussed in Section 3. The linear stability analysis and PES condition are explored in Section 4. Section 5 contains the details of the nonlinear analysis and the corresponding main transition theorem. In Section 6 we present results obtained through numerical simulations and the conclusions that can be extracted from them in combination with the main transition theorem.

2. Governing equations

The two dimensional Boussinesq equations describing a fluid with internal heating, varying gravity, L-periodicity in the x-direction, and y-homogeneity are given by

$$\begin{aligned} &\frac{\partial \mathbf{u}}{\partial t} + (\mathbf{u}\cdot\nabla)\mathbf{u} + \frac{1}{\rho_0}\nabla P = \nu\Delta\mathbf{u} + \alpha\mathbf{k}g(z)T, \\ &\frac{\partial T}{\partial t} + (\mathbf{u}\cdot\nabla)T = \kappa\Delta T + Q(z), \\ &\text{div } \mathbf{u} = 0, \end{aligned} \tag{2.1}$$

supplemented with the boundary conditions

$$\mathbf{u}(x+L,z) = \mathbf{u}(x,z), \qquad T(x+L,z) = T(x,z), \tag{2.2}$$

$$\mathbf{u}(x,0) = \mathbf{u}(x,h) = \mathbf{0}, \qquad \frac{\partial T}{\partial z}(x,0) = 0, \quad T(x,h) = 0. \tag{2.3}$$

The function $Q(z)$ in the second equation of system (2.1) is a generic heating source. We assume the gravitational potential term g above is of the form

$$g(z) = g_0(1 + l(z))$$

where g_0 is a constant and $l(z)$ is a dimensionless function of the height.

It can be verified by direct substitution that a simple steady state solution of the above equations is given by

$$\begin{aligned} &\bar{\mathbf{u}} \equiv \mathbf{0}, \quad \bar{T}(z) = -\frac{1}{\kappa}\int_0^z (z - z')Q(z')dz' - cz, \\ &\bar{P}(z) = -\rho_0 \int_0^z g(z')\left(1 - \alpha(\bar{T}(z'))\right)dz', \end{aligned} \tag{2.4}$$

where the constant c is given by

$$c = -\frac{1}{\kappa h}\int_0^h (h - z)Q(z)dz.$$

In order to make the equations describing deviations from this steady state non-dimensional, we let

$$\begin{aligned} &(\mathbf{x}, t) = \left(h\mathbf{x}', \frac{h^2}{\nu}t'\right), \\ &(\mathbf{u}, T, P) = \left(\nu\mathbf{u}'/h, \bar{T} + \left(\frac{c\nu^3}{\kappa g_0 \alpha h^2}\right)^{1/2}\theta', \bar{P} + \frac{\rho_0\nu^2}{h^2}P'\right), \\ &N'(z) = \frac{1}{\kappa c}\int_0^z Q(z')dz', \qquad H'(z) = 1 + l(z) = \frac{g(z)}{g_0}, \\ &\text{Pr} = \nu/\kappa, \qquad \gamma = \frac{L}{h}, \qquad R = \left(\frac{ch^4 g_0 \alpha}{\kappa\nu}\right)^{\frac{1}{2}}. \end{aligned}$$

We recall that Pr is the Prandtl number, γ is the aspect ratio, and R is the Rayleigh number.

Then, omitting the primes and setting $\mathbf{u}=(u,w)$, we can write the resulting equations as

$$\begin{aligned}
&\frac{\partial u}{\partial t}+(\mathbf{u}\cdot\nabla)u+\frac{\partial P}{\partial x}=\Delta u\\
&\frac{\partial w}{\partial t}+(\mathbf{u}\cdot\nabla)w+\frac{\partial P}{\partial z}=\Delta w+RH(z)\theta,\\
&\Pr\left(\frac{\partial \theta}{\partial t}+(\mathbf{u}\cdot\nabla)\theta\right)=\Delta\theta+RN(z)w,\\
&\frac{\partial u}{\partial x}+\frac{\partial w}{\partial z}=0.
\end{aligned} \tag{2.5}$$

The boundary conditions are non-dimensionalized accordingly as well.

Throughout this article it is assumed that H and N are smooth with bounded derivatives of all orders. In our numerical simulations we will further restrict our attention to the following expressions of H and N, taken from [14],

$$H(z)=1+\delta z,\qquad \delta\in[0,1], \tag{2.6}$$

$$N(z)=\begin{cases}
N_1(z)=z,\\
N_2(z)=\dfrac{1}{2}(z+z^2),\\
N_3(z)=2z+\dfrac{1}{2}z^3-\dfrac{3}{2}z^2,\\
N_4(z)=\dfrac{1}{2\pi}\left(1-\cos(2\pi z)\right),\\
N_5(z)=e^z-1-z,\\
N_6(z)=z+\dfrac{1}{4\pi}(3-2\cos 2\pi z-\cos 4\pi z),
\end{cases} \tag{2.7}$$

These terms N are selected to represent a wide range of heating sources and sinks. Specifically, N is a heating source if its derivative is positive; N is a sink if its derivative is negative; and N is mixed if its derivative changes sign, see Figure 2.1 for an illustration.

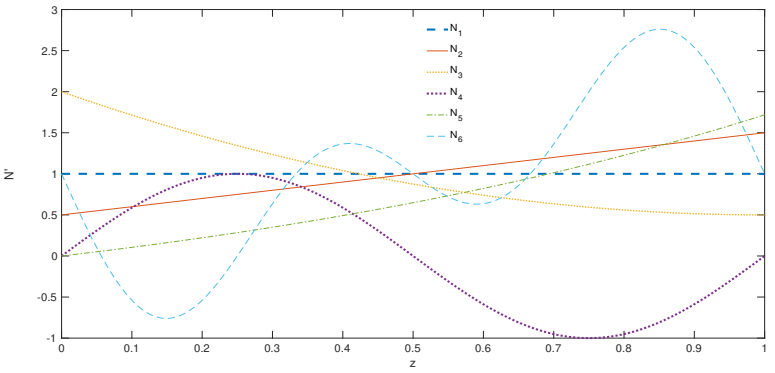

Fig. 2.1: *The derivative of N, which is a source (sink) if it is positive (negative); N is mixed if its derivative changes sign.*

3. Mathematical formulation

The forthcoming analysis is considerably simplified by using instead a stream-function formulation of (2.5). This is accomplished by setting $u=\dfrac{\partial\psi}{\partial z}$ and $w=-\dfrac{\partial\psi}{\partial x}$. The resulting equations then take the form

$$\begin{cases}\dfrac{\partial}{\partial t}\Delta\psi=\Delta^2\psi-RH(z)\dfrac{\partial\theta}{\partial x}+J(\psi,\Delta\psi),\\ \mathrm{Pr}\dfrac{\partial\theta}{\partial t}=\Delta\theta-RN(z)\dfrac{\partial\psi}{\partial x}+\mathrm{Pr}J(\psi,\theta),\end{cases}\tag{3.1}$$

where

$$J(u,v)=\frac{\partial u}{\partial x}\frac{\partial v}{\partial z}-\frac{\partial u}{\partial z}\frac{\partial v}{\partial x}.$$

Furthermore, the corresponding domain Ω and boundary conditions are now

$$\Omega=(0,\gamma)\times(0,1),\tag{3.2}$$

$$\psi(x+\gamma,z)=\psi(x,z),\quad \theta(x+\gamma,z)=\theta(x,z),\tag{3.3}$$

$$\psi(x,0)=\psi(x,1)=\frac{\partial\psi}{\partial z}(x,0)=\frac{\partial\psi}{\partial z}(x,1)=0,\tag{3.4}$$

$$\theta(x,1)=\frac{\partial\theta}{\partial z}(x,0)=0.\tag{3.5}$$

In what follows we formulate the evolution equations given in (3.1) using an abstract functional setting that is standard in the framework of dynamic transitions.

First, we let $H^4(\Omega)$, $H^2(\Omega)$, and $L^2(\Omega)$ denote the usual Sobolev and Lebesgue spaces. Then, denoting $\varphi=(\psi,\theta)$, we let H_1, H_0 and H_{-1} be the Hilbert spaces given by

$$\begin{aligned}H_1&=\{\varphi\in H^4(\Omega)\times H^2(\Omega)|\ \varphi \text{ satisfies } (3.3)-(3.5)\},\\ H_0&=\{\varphi\in H^2(\Omega)\times L^2(\Omega)|\ \varphi \text{ satisfies } (3.3)-(3.4)\},\\ H_{-1}&=\{\varphi\in L^2(\Omega)^2|\ \varphi \text{ satisfies } (3.3)\},\end{aligned}$$

endowed with their natural inner products.

We can then introduce differential operators $\mathcal{L}_R,\mathcal{G}:H_1\to H_{-1}$ and $\mathcal{A}:H_0\to H_{-1}$ as follows

$$\mathcal{L}_R\varphi=\begin{pmatrix}\Delta^2\psi-RH(z)\frac{\partial\theta}{\partial x}\\ \Delta\theta-RN(z)\frac{\partial\psi}{\partial x}\end{pmatrix},\tag{3.6}$$

$$\mathcal{G}(\varphi)=\begin{pmatrix}J(\psi,\Delta\psi)\\ \mathrm{Pr}J(\psi,\theta)\end{pmatrix},\qquad \mathcal{A}\varphi=\begin{pmatrix}\Delta\psi\\ \mathrm{Pr}\theta\end{pmatrix}\tag{3.7}$$

We thus obtain the following equivalent form of (3.1)

$$\frac{d}{dt}\mathcal{A}\varphi=\mathcal{L}_R\varphi+\mathcal{G}(\varphi).\tag{3.8}$$

Note that $\mathcal{A}$ is an isomorphism between H_0 and $\mathcal{A}(H_0)\subset H_{-1}$, and $\mathcal{L}(H_1)\subset\mathcal{A}(H_0)$, hence the operator $L_R:=\mathcal{A}^{-1}\circ\mathcal{L}_R$ is bounded from H_1 into H_0. Furthermore, due to the classical Sobolev embeddings, the inclusion $H_1\hookrightarrow H_0$ is dense and compact, and thus $L_R: D(L_R)=H_1\subset H_0\to H_0$ has a compact resolvent.

Similar considerations regarding the spectrum of L_R, and the continuity of the quadratic form G, allow us to cast this problem in the form

$$\begin{cases} \dfrac{du}{dt} = L_R u + G(u), \\ u(0) = u_0 \in H_0, \end{cases} \tag{3.9}$$

and show that it satisfies the hypotheses of [17] p. 41.

4. Linear analysis

As is customary in the theory of dynamical systems, we begin by studying the linearized equations associated with (3.1). They take the form of a generalized eigenvalue problem,

$$\mathcal{L}_R \varphi = \beta \mathcal{A} \varphi.$$

Noting that $\mathcal{A}$ is self-adjoint, we see that the corresponding dual equations are

$$\mathcal{L}_R^* \varphi^* = \beta^* \mathcal{A} \varphi^*.$$

where the same boundary conditions (3.3) and (3.4) are in place.

These eigenvalue problems have the important property that their solutions are orthogonal under the inner product $\langle \mathcal{A}\cdot, \cdot \rangle$. That is, if β is a simple eigenvalue with corresponding eigenfunction φ, and (β', φ^*) is a solution of the dual problem, then

$$\langle \mathcal{A}\varphi, \varphi^* \rangle \neq 0 \Longleftrightarrow \beta' = \overline{\beta}, \tag{4.1}$$

where $\overline{\beta}$ denotes the complex conjugate of β.

Except for very special cases (c.f. Appendix), the aforementioned eigenvalue problem does not possess a closed form solution. Consequently, we approach this problem by using a numerical scheme as follows. First, by taking advantage of the periodicity on the horizontal direction, we use the method of separation of variables to write

$$\begin{aligned} \psi(x,z) &= e^{ia_m x} \Psi(z), \\ \theta(x,z) &= e^{ia_m x} \Theta(z), \end{aligned} \tag{4.2}$$

where $a_m = \frac{2\pi m}{\gamma}$.

Next we introduce the family of one-dimensional differential operators given by

$$\begin{aligned} \mathcal{A}_m(\Psi, \Theta) &= \begin{pmatrix} (\partial_z^2 - a_m^2)\Psi \\ Pr\Theta \end{pmatrix}, \\ \mathcal{L}_m(\Psi, \Theta) &= \begin{pmatrix} (\partial_z^2 - a_m^2)^2 \Psi - i a_m R H(z) \Theta \\ (\partial_z^2 - a_m^2)\Theta - i a_m R N(z) \Psi \end{pmatrix}. \end{aligned}$$

Then the eigenfunctions can be determined by solving the following family of boundary value problems:

$$\begin{cases} \mathcal{L}_m(\Psi_{m,k}, \Theta_{m,k}) = \beta_{m,k} \mathcal{A}_m(\Psi_{m,k}, \Theta_{m,k}), \\ \Psi_{m,k}(0) = \left. \dfrac{d\Psi_{m,k}}{dz} \right|_{z=0} = 0, \\ \Psi_{m,k}(1) = \left. \dfrac{d\Psi_{m,k}}{dz} \right|_{z=1} = 0, \\ \left. \dfrac{d\Theta_{m,k}}{dz} \right|_{z=0} = \Theta_{m,k}(1) = 0. \end{cases} \tag{4.3}$$

Without loss of generality we assume that the eigenvalues $\{\beta_{m,k}\}_{m,k}$ are ordered by decreasing real part for each wavenumber. That is, we assume that

$$\Re\beta_{m,1} \geq \Re\beta_{m,2} \geq \Re\beta_{m,3} \geq \cdots \to -\infty, \qquad \forall m \in \mathbb{Z}.$$

Then the principle of exchange of stabilities (PES condition) takes the following form:

DEFINITION 4.1 (Principle of Exchange of Stabilities). *There exists $n \in \mathbb{Z}\setminus\{0\}$ and $R^* > 0$ such that, for all R close enough to R^*,*

$$\Re\beta_{n,1} \begin{cases} > 0 & \text{if } R > R^*, \\ = 0 & \text{if } R = R^*, \\ < 0 & \text{if } R < R^*, \end{cases} \tag{4.4}$$

$$\Re\beta_{m,k} < 0 \quad \text{if } m \neq n \text{ or } k > 1. \tag{4.5}$$

It is known that the PES holds for this problem for almost every value of γ, see e.g. [15, 16]. Hereafter we will proceed under the working assumption that the wavenumber m has been chosen to satisfy this condition. More precisely, we will study the transition as R crosses R^*, for $\gamma \in [1, 10]$.

The solution to the eigenvalue problem is obtained using a classical spectral Galerkin numerical scheme, see [18] for details. Below we show the components of the eigenfunction corresponding to the heating source $N(z) = N_4(z) = \frac{1}{2\pi}(1 - \cos(2\pi z))$; other choices of N give rise to qualitatively similar results, with the differences being mostly confined to the shape of the θ profiles. For the purpose of illustration we take $\gamma = 8$, where the PES holds for $n = 3$ and the critical Rayleigh number is given approximately by $R^* = 73.175136$. Note that the real and imaginary parts of the associated eigenfunctions in Figure 4.1 differ only by a translation in the horizontal direction.

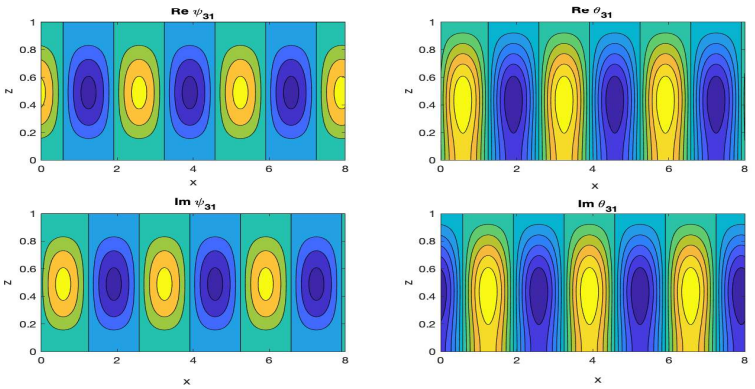

Fig. 4.1: *Eigenfunction corresponding to $n = 3$ and $k = 1$, with $\gamma = 8$ and $N(z) = N_4$.*

As mentioned above, we also explore the values of the critical Rayleigh number from a global perspective. More precisely, we compute for each $\gamma > 0$ the value R_m of R such that $\max_k \Re\beta_{m,k} = 0$. By doing this we obtain, for each m, a curve $R_m = R_m(\gamma)$ that determines the onset of linear instability for each wavenumber.

Furthermore, for all but countably many values of γ, there is only one wavenumber $n = n(\gamma)$ for which $R_n = \min_{m\in\mathbb{N}} R_m^*$. Thus, this is the critical Rayleigh number $R^* = R_n$

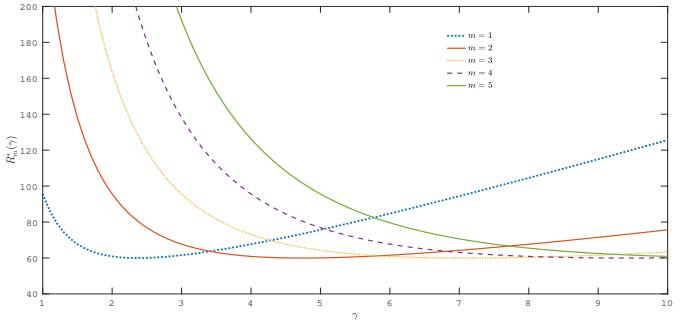

Fig. 4.2: *Neutral stability curves for a given wavenumber,* $R=R^*_m(\gamma)$, *i.e. the roots of* $\max_k \Re\beta_{m,k}(\gamma,R)=0$.

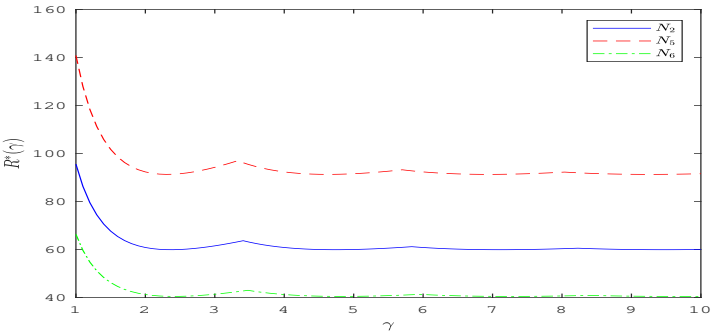

Fig. 4.3: *Neutral stability curves,* $R=R^*(\gamma)$, *i.e. the roots of* $\min_{m,k} \Re\beta_{m,k}(\gamma,R)=0$.

at which the first transition occurs. This defines a continuous function $R=R^*(\gamma)$ that is piecewise smooth, with possible cusp points at the values of γ for which there is more than one wavenumber giving rise to linear instability – or, equivalently, the center subspace has dimension greater than 2.

In Figure 4.2 we show the curves $R^*_m=R^*_m(\gamma)$ for different values of m for a special heating source $(N(z)=z)$. Note that the critical wavenumber n increases with the aspect ratio parameter γ.

The critical Rayleigh number, as discussed above, is then given by $R^*=\min_{m\in\mathbb{N}} R^*_m$, and can be easily obtained from the previous analysis. We show in Figure 4.3 the associated curves $R=R^*(\gamma)$ for an ensemble of different heating sources. We made numerical simulations for all the different heating sources mentioned in the previous section, but the results were all qualitatively identical. Thus, for the purpose of illustration, we only show here three of them, which we note differ only in amplitude and the exact location of the cusps that occur when the heating source N changes.

5. Reduced equations and main theorem

Let us denote the center-unstable space by H_c. That is, H_c is given by the real part of the complex linear span of all the eigenfunctions with the real part of corresponding eigenvalue changing its sign at critical Rayleigh number R^*. We similarly denote by H^*_c the center-unstable subspace associated with the dual eigenvalue problem.

Because of the previous discussion we know that, generically, H_c and H^*_c have

dimension 2 and are respectively given by the real part of the complex span of

$$\varphi_1(x,z)=\begin{pmatrix}\psi_1(x,z)\\ \theta_1(x,z)\end{pmatrix}=e^{ia_nx}\begin{pmatrix}\Psi_1(z)\\ \Theta_1(z)\end{pmatrix}, \tag{5.1}$$

$$\varphi_1^*(x,z)=\begin{pmatrix}\psi_1^*(x,z)\\ \theta_1^*(x,z)\end{pmatrix}=e^{ia_nx}\begin{pmatrix}\Psi_1^*(z)\\ \Theta_1^*(z)\end{pmatrix}, \tag{5.2}$$

where the wavenumber n above is chosen so that

$$\Re\beta_{n,1}=\max_{m,k}\Re\beta_{m,k}.$$

Upon choosing a normalization for φ_1 above, any element φ in H_c can be written uniquely in the form

$$\varphi=\zeta\varphi_1+\overline{\zeta\varphi_1}, \tag{5.3}$$

for some $\zeta\in\mathbb{C}$. An analogous property holds for φ_1^* and H_c^*.

Thus, the approximate expression for the center manifold given by (A.2.12) in [17] takes the form

$$h(\varphi)=h_2(\varphi)+o(|\zeta|^2). \tag{5.4}$$

Here h_2 is the quadratic leading order approximation of the center manifold function, which is uniquely determined by the equations

$$2\beta\mathcal{A}h_2(\varphi)-\mathcal{L}_Rh_2(\varphi)=\mathcal{G}(\varphi,\varphi)=\zeta^2\mathcal{G}(\varphi_1,\varphi_1)+\overline{\zeta}^2\mathcal{G}(\overline{\varphi_1},\overline{\varphi_1})+|\zeta|^2(\mathcal{G}(\varphi_1,\overline{\varphi_1})+\mathcal{G}(\overline{\varphi_1},\varphi_1)). \tag{5.5}$$

where we recall the bilinear form $\mathcal{G}(u,v)$ is given by

$$\mathcal{G}(u,v)=\begin{pmatrix}J(u_1,\Delta v_1)\\ \mathrm{Pr}J(u_1,v_2)\end{pmatrix},u=\begin{pmatrix}u_1\\ u_2\end{pmatrix},v=\begin{pmatrix}v_1\\ v_2\end{pmatrix}. \tag{5.6}$$

Upon substituting (5.1) in (5.6) we find that

$$\mathcal{G}(\varphi_1,\varphi_1)(x,z)=ia_ne^{i2a_nx}\begin{pmatrix}\Psi_1(z)\Psi_1'''(z)-\Psi_1'(z)\Psi_1''(z)\\ \mathrm{Pr}\Psi_1(z)\Theta_1'(z)-\mathrm{Pr}\Psi_1'(z)\Theta_1(z)\end{pmatrix}, \tag{5.7}$$

$$\mathcal{G}(\overline{\varphi_1},\overline{\varphi_1})(x,z)=-ia_ne^{-i2a_nx}\begin{pmatrix}\overline{\Psi_1(z)\Psi_1'''(z)}-\overline{\Psi_1'(z)\Psi_1''(z)}\\ \mathrm{Pr}\overline{\Psi_1(z)\Theta_1'(z)}-\mathrm{Pr}\overline{\Psi_1'(z)\Theta_1(z)}\end{pmatrix}. \tag{5.8}$$

$$\begin{aligned}\mathcal{G}(\varphi_1,\overline{\varphi_1})(x,z)=&ia_n\begin{pmatrix}\Psi_1(z)\overline{\Psi_1}'''(z)+\Psi_1'(z)\overline{\Psi_1}''(z)\\ \mathrm{Pr}\Psi_1(z)\overline{\Theta_1'(z)}\end{pmatrix}\\ &-ia_n\begin{pmatrix}a_n^2\Psi_1'(z)\overline{\Psi_1(z)}+a_n^2\Psi_1(z)\overline{\Psi_1'(z)}\\ -\mathrm{Pr}\Psi_1'(z)\overline{\Theta_1(z)}\end{pmatrix},\\ \mathcal{G}(\overline{\varphi_1},\varphi_1)(x,z)=&ia_n\begin{pmatrix}a_n^2\overline{\Psi_1'(z)}\Psi_1(z)+a_n^2\overline{\Psi_1(z)}\Psi_1'(z)\\ -\mathrm{Pr}\overline{\Psi_1(z)}\Theta_1'(z)\end{pmatrix}\\ &-ia_n\begin{pmatrix}\overline{\Psi_1(z)}\Psi_1'''(z)+\overline{\Psi_1'(z)}\Psi_1''(z)\\ \mathrm{Pr}\overline{\Psi_1'(z)}\Theta_1(z)\end{pmatrix},\end{aligned} \tag{5.9}$$

and

$$[\mathcal{G}(\varphi_1,\overline{\varphi_1})+\mathcal{G}(\overline{\varphi_1},\varphi_1)](x,z)=ia_n\begin{pmatrix}\Psi_1(z)\overline{\Psi_1'''(z)}+\Psi_1'(z)\overline{\Psi_1''(z)}\\ \mathrm{Pr}\Psi_1(z)\overline{\Theta_1'(z)}+\mathrm{Pr}\Psi_1'(z)\overline{\Theta_1(z)}\end{pmatrix}$$
$$-ia_n\begin{pmatrix}\overline{\Psi_1(z)}\Psi_1'''(z)+\overline{\Psi_1'(z)}\Psi_1''(z)\\ \mathrm{Pr}\overline{\Psi_1'(z)}\Theta_1(z)+\mathrm{Pr}\overline{\Psi_1(z)}\Theta_1'(z)\end{pmatrix}. \tag{5.10}$$

Note that $\mathcal{A}$ and $\mathcal{L}_R$ are linear operators. Then the right-hand side of the Equation (5.5) allows us to look for its solution $h_2(\phi)$ in the form of

$$h_2(\phi)=\zeta^2\varphi_{20}+|\zeta|^2\varphi_{11}+\overline{\zeta}^2\varphi_{02}.$$

Inserting the preceding formula into (5.5) and comparing coefficients on both sides, we obtain a system of equations for the coefficients $\varphi_{20},\varphi_{11},\varphi_{02}$ given by

$$\begin{aligned}&2\beta\mathcal{A}\varphi_{20}-\mathcal{L}_R\varphi_{20}=\mathcal{G}(\varphi_1,\varphi_1),\\ &2\overline{\beta}\mathcal{A}\varphi_{02}-\mathcal{L}_R\varphi_{02}=\mathcal{G}(\overline{\varphi_1},\overline{\varphi_1}),\\ &2\Re\beta\mathcal{A}\varphi_{11}-\mathcal{L}_R\varphi_{11}=\mathcal{G}(\varphi_1,\overline{\varphi_1})+\mathcal{G}(\overline{\varphi_1},\varphi_1).\end{aligned} \tag{5.11}$$

Noting that the x dependence on the right-hand side of (5.11) involves, at most, only terms of the form $e^{\pm 2ia_nx}$, we can again use separation of variables to write

$$\varphi_{20}(x,z)=\begin{pmatrix}\psi_{20}(x,z)\\ \theta_{20}(x,z)\end{pmatrix}=e^{2ia_nx}\begin{pmatrix}\Psi_{20}(z)\\ \Theta_{20}(z)\end{pmatrix}, \tag{5.12}$$

$$\varphi_{02}(x,z)=\begin{pmatrix}\psi_{02}(x,z)\\ \theta_{02}(x,z)\end{pmatrix}=e^{-2ia_nx}\begin{pmatrix}\Psi_{02}(z)\\ \Theta_{02}(z)\end{pmatrix}, \tag{5.13}$$

$$\varphi_{11}(x,z)=\begin{pmatrix}\psi_{11}(x,z)\\ \theta_{11}(x,z)\end{pmatrix}=\begin{pmatrix}\Psi_{11}(z)\\ \Theta_{11}(z)\end{pmatrix}. \tag{5.14}$$

Furthermore, since the quadratic form $\mathcal{G}$ has no complex-valued coefficients, it follows from (5.7)–(5.8) and (5.11) that

$$\varphi_{20}=\overline{\varphi_{02}}.$$

Hence, we only need to solve the first and third equations in (5.11), which, upon using (5.12)-(5.14), take the form

$$\begin{cases}(2\beta_{n,1}\mathcal{A}_{2n}-\mathcal{L}_{2n})(\Psi_{20},\Theta_{20})=e^{-2ia_nx}\mathcal{G}(\varphi_1,\varphi_1),\\ (2\Re\beta_{n,1}\mathcal{A}_0-\mathcal{L}_0)(\Psi_{11},\Theta_{11})=\mathcal{G}(\varphi_1,\overline{\varphi_1})+\mathcal{G}(\overline{\varphi_1},\varphi_1),\\ \Psi_{20}(0)=\Psi_{11}(0)=\dfrac{d\Psi_{20}}{dz}\Big|_{z=0}=\dfrac{d\Psi_{11}}{dz}\Big|_{z=0}=0,\\ \Psi_{20}(1)=\Psi_{11}(1)=\dfrac{d\Psi_{20}}{dz}\Big|_{z=1}=\dfrac{d\Psi_{11}}{dz}\Big|_{z=1}=0,\\ \dfrac{d\Theta_{20}}{dz}\Big|_{z=0}=\dfrac{d\Theta_{11}}{dz}\Big|_{z=0}=\Theta_{20}(1)=\Theta_{11}(1)=0.\end{cases}$$

At this point no further analytical simplifications are possible in this generality, and the problem must be approached through a numerical scheme. Nevertheless, assuming the coefficients φ_{ij} have been found we can continue the analysis from an abstract perspective.

Applying the general formula for the reduced equations (A.2.12) in [17], we obtain the complex-valued ODE

$$\frac{d\zeta}{dt} = \beta_{n,1}\zeta + \langle \mathcal{G}(\varphi,\varphi) + \mathcal{G}(\varphi,h_2) + \mathcal{G}(h_2,\varphi), \varphi_1^* \rangle + o(|\zeta|^3), \tag{5.15}$$

where we use the normalization

$$\langle \mathcal{A}\varphi_1, \varphi_1^* \rangle = \frac{1}{\gamma}\int_\Omega \mathcal{A}\varphi_1 \overline{\varphi_1^*} d\mathbf{x} = 1.$$

Combining (5.3) and (5.4) we find that

$$\begin{aligned}
\langle \mathcal{G}(\varphi,h_2),\varphi_1^* \rangle =& \langle \mathcal{G}(\zeta\varphi_1 + \overline{\zeta\varphi_1}, \zeta^2\varphi_{20} + |\zeta|^2\varphi_{11} + \overline{\zeta}^2\varphi_{02}), \varphi_1^* \rangle \\
=& \zeta^3 \langle \mathcal{G}(\varphi_1,\varphi_{20}),\varphi_1^*\rangle + \zeta|\zeta|^2\langle \mathcal{G}(\overline{\varphi_1},\varphi_{20}),\varphi_1^*\rangle \\
&+ \zeta|\zeta|^2\langle \mathcal{G}(\varphi_1,\varphi_{11}),\varphi_1^*\rangle + \overline{\zeta}|\zeta|^2\langle \mathcal{G}(\overline{\varphi_1},\varphi_{11}),\varphi_1^*\rangle \\
&+ \overline{\zeta}|\zeta|^2\langle \mathcal{G}(\varphi_1,\varphi_{02}),\varphi_1^*\rangle + \overline{\zeta}^3\langle \mathcal{G}(\overline{\varphi_1},\varphi_{02}),\varphi_1^*\rangle,
\end{aligned}$$

$$\begin{aligned}
\langle \mathcal{G}(h_2,\varphi),\varphi_1^* \rangle =& \langle \mathcal{G}(\zeta^2\varphi_{20} + |\zeta|^2\varphi_{11} + \overline{\zeta}^2\varphi_{02}, \zeta\varphi_1 + \overline{\zeta\varphi_1}), \varphi_1^* \rangle \\
=& \zeta^3 \langle \mathcal{G}(\varphi_{20},\varphi_1),\varphi_1^*\rangle + \zeta|\zeta|^2\langle \mathcal{G}(\varphi_{20},\overline{\varphi_1}),\varphi_1^*\rangle \\
&+ \zeta|\zeta|^2\langle \mathcal{G}(\varphi_{11},\varphi_1),\varphi_1^*\rangle + \overline{\zeta}|\zeta|^2\langle \mathcal{G}(\varphi_{11},\overline{\varphi_1}),\varphi_1^*\rangle \\
&+ \overline{\zeta}|\zeta|^2\langle \mathcal{G}(\varphi_{02},\varphi_1),\varphi_1^*\rangle + \overline{\zeta}^3\langle \mathcal{G}(\varphi_{02},\overline{\varphi_1}),\varphi_1^*\rangle,
\end{aligned}$$

The above can be further simplified by making use of (5.1)–(5.2) and (5.13)–(5.14), from where one can see that

$$\begin{aligned}
\langle \mathcal{G}(\varphi_1,\varphi_{20}),\varphi_1^*\rangle = \langle \mathcal{G}(\varphi_{20},\varphi_1),\varphi_1^*\rangle = 0, \\
\langle \mathcal{G}(\overline{\varphi_1},\varphi_{11}),\varphi_1^*\rangle = \langle \mathcal{G}(\varphi_{11},\overline{\varphi_1}),\varphi_1^*\rangle = 0, \\
\langle \mathcal{G}(\varphi_1,\varphi_{02}),\varphi_1^*\rangle = \langle \mathcal{G}(\varphi_{02},\varphi_1),\varphi_1^*\rangle = 0, \\
\langle \mathcal{G}(\overline{\varphi_1},\varphi_{02}),\varphi_1^*\rangle = \langle \mathcal{G}(\varphi_{02},\overline{\varphi_1}),\varphi_1^*\rangle = 0.
\end{aligned}$$

Hence, letting $P \in \mathbb{C}$ be given by

$$\begin{aligned}
P =& \langle \mathcal{G}(\overline{\varphi_1},\varphi_{20}),\varphi_1^*\rangle + \langle \mathcal{G}(\varphi_1,\varphi_{11}),\varphi_1^*\rangle \\
&+ \langle \mathcal{G}(\varphi_{20},\overline{\varphi_1}),\varphi_1^*\rangle + \langle \mathcal{G}(\varphi_{11},\varphi_1),\varphi_1^*\rangle.
\end{aligned} \tag{5.16}$$

we see that the reduced Equations (5.15) take the form

$$\frac{d\zeta}{dt} = \beta_{n,1}\zeta + P\zeta|\zeta|^2 + o(|\zeta|^3). \tag{5.17}$$

In what follows we refer to P above as the transition number, since the sign of its real part completely determines the type of transition. Although above calculations show that P is always a real number in this problem, its exact value can only be determined numerically in the general case. Nevertheless, in the special case of constant N and H, and with slightly different boundary conditions, we are able to obtain a closed form formula for P (c.f. Appendix).

From the preceding discussion we see that the type of transition for the problem (3.1) is completely determined by the reduced Equations (5.15). More precisely, the

sign of P given in (5.16) determines which of the three different types of transitions from the basic solution (2.4) can occur. We summarize these results in the following:

THEOREM 5.1. *If $P<0$, then (3.1) undergoes a continuous transition at the critical Rayleigh number R^*. More precisely,*

- *If the Rayleigh number $R<R^*$, the steady state $(\psi,\theta)=(0,0)$ is locally asymptotically stable.*
- *The problem (3.1) bifurcates from $((0,0),R^*)$ to an attractor $\mathcal{B}$ homeomorphic to $\mathbb{S}^1$ which consists of infinitely many steady states. In addition, any $(\psi,\theta)\in\mathcal{B}$ can be expressed as*

$$(\psi,\theta)=\left(\frac{\beta_{n,1}}{|P|}\right)^{\frac{1}{2}}(x\Re\varphi_1+y\Im\varphi_1)+o\left(\left(\frac{\beta_{n,1}}{|P|}\right)^{\frac{1}{2}}\right),\qquad x^2+y^2=1.$$

- *There is an open set $U\in H_1$ such that $\mathcal{B}$ attracts $U\setminus\Gamma$, where Γ is the stable manifold of the origin, which has codimension 2 in H_1.*

Proof. By the $\mathbb{S}^1$ attractor bifurcation theorem (see Theorem 2.2.3 in [17]), we only need to show that the origin is a locally stable equilibrium point when $R=R^*$, and that there exists a family of steady states which are homeomorphic to S^1.

Using (5.17) we see that $r=|\zeta|$ satisfies the ODE

$$\frac{dr}{dt}=\Re\beta_{n,1}(R)r+Pr^3+o(r^3). \tag{5.18}$$

When $R=R^*$ we have $\Re\beta_{n,1}(R)=0$ and $P<0$, and thus the solution $r(t)$ of the preceding equation with any sufficiently small initial value r_0 decreases to zero as t increases, i.e., the origin is a locally stable equilibrium point for the reduced Equation (5.17). Hence, the origin is a locally stable equilibrium point for (3.1) at $R=R^*$.

Let now $\varphi_s(x,z)$ be any steady state of (3.1) which is nonconstant. It can be directly verified that the problem (3.1), subject to (3.3)-(3.4), is invariant under the transformation

$$\varphi_s(x,z)\to\varphi_s(x+x_0,z),\forall x_0\in R.$$

Then, letting

$$\Sigma_s=\{\varphi_s(x+x_0,z)|\forall x_0\in R\},$$

it is clear that Σ_s is homeomorphic to S^1. The proof is complete. ∎

REMARK 5.1. A similar result, albeit rather more complicated to formulate, holds in the complementary case $P>0$, which corresponds to a jump transition. However, as shown below, our numerical simulations suggest that this scenario can never occur for this system. Thus Theorem 5.1 completely characterizes the transition type of this problem.

6. Numerical results

As discussed in the preceding section, the transition that (3.1) undergoes at the critical Rayleigh number R^* can only be of continuous or catastrophic type. In this section, we find using numerical experiments the exact type of transition for (3.1) under the effect of six different heating sources N taken from [14]. In particular, we analyze the functional dependence between the transition number P and the geometric parameter γ.

It is clear that the first eigenfunction and the corresponding dual eigenfunction can only be computed numerically. For this purpose we rely on the classical spectral Galerkin Legendre method. The details of such a procedure are well known, and a more detailed discussion can be found in [18].

First, we make a comparison between the exact transition number and its numerical counterpart to show that our implementation of the method is highly accurate when predicting the value of P. In order to do this, we focus on the case when H and N in (3.1) are constants, and use slightly different boundary conditions (7.1)–(7.2). The exact formula for the transition number $P=P_0$ is given in the Appendix.

Table 6.1: Comparison between exact values of transition number and numerical predictions.

H,N,γ	Exact P	Numerical prediction	Relative error
$H=1,N=1,\gamma=2$	-0.237945538212927	-0.237945538209306	1.52×10^{-11}
$H=1,N=2,\gamma=2$	-0.121911934621018	-0.121911934619325	1.39×10^{-11}
$H=1,N=1,\gamma=3$	-0.143761912015905	-0.143761912018452	1.77×10^{-11}
$H=1,N=2,\gamma=3$	-0.074316592089502	-0.074316592086761	3.69×10^{-11}

As seen in the above table, this method works as a good predictor of the sign of the transition number as long as the predicted value is at least 10^{-11} away from zero. Note also that, under these boundary conditions, the type of transition for the Rayleigh-Bénard convection problem is always continuous.

The goal in the following is to study the transition type for the six different heating sources given by (2.6) for different values of the ratio aspect γ. For all our simulations we take $\delta=\frac{1}{100}$, $Pr=10$, and let γ take values in the interval $[1,10]$. We recall that these heating sources are given by

$$N(z)=\begin{cases} N_1(z)=z, \\ N_2(z)=\dfrac{1}{2}(z+z^2), \\ N_3(z)=2z+\dfrac{1}{2}z^3-\dfrac{3}{2}z^2, \\ N_4(z)=\dfrac{1}{2\pi}\left(1-\cos(2\pi z)\right), \\ N_5(z)=e^z-1-z, \\ N_6(z)=z+\dfrac{1}{4\pi}(3-2\cos 2\pi z-\cos 4\pi z), \end{cases} \tag{6.1}$$

The corresponding values of P are shown in Figure 6.1, and the critical Rayleigh numbers are shown in Figure 4.3. For the sake of clarity we show only values of P associated with $N(z)=N_i(z)$ for $i=2,5,6$; other heating sources give rise to very similar results.

As seen in Figure 6.1, the sign of P is always negative, which remains true for all six different heating sources. Thus, the corresponding types of dynamic transitions are always continuous. Physically, this means that the critical Rayleigh numbers for different aspect ratios found using linear stability analysis will also coincide with the values measured experimentally.

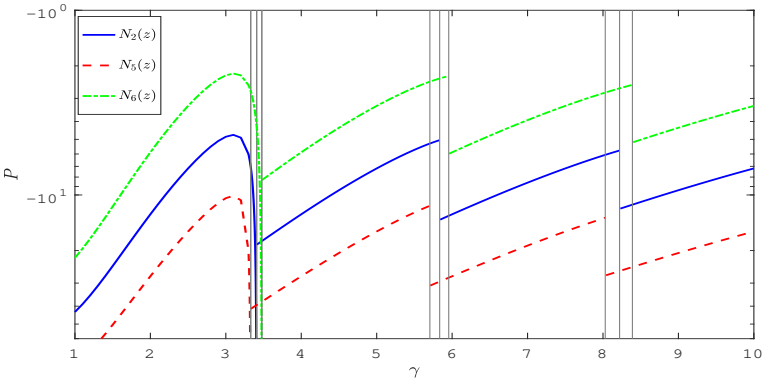

Fig. 6.1: *The transition number P given in (5.16) for different heating sources and for Prandtl number $Pr=10$*

From Figure 6.1 we see that the transition number P is discontinuous as a function of the aspect ratio γ. In fact, as Figures 6.1 and 4.3 show, the left and right limits of P differ exactly at the values of γ at which the first eigenvalue has algebraic multiplicity greater than one. Furthermore, recalling that, from Theorem 5.1, the approximate expression of a bifurcated steady state solution of (3.1) for $R>R^*$ is

$$\mathbf{U}_s=(\psi,\theta)=\left(\frac{\beta_{n,1}}{|P|}\right)^{\frac{1}{2}}(x\Re\varphi_1+y\Im\varphi_1)+o\left(\left(\frac{\beta_{n,1}}{|P|}\right)^{\frac{1}{2}}\right),\quad x^2+y^2=1, \tag{6.2}$$

we see that the map $\gamma\mapsto\mathbf{U}_s$ inherits these discontinuities.

In order to gain more insight into the topological meaning of this phenomenon, we turn to (7.3). In this special case, since we have an explicit formula, it is clear that the transition number, P_0, depends on γ only through $a_n=\frac{2n\pi}{\gamma}$, and there exists an increasing sequence $\{\gamma_i\}_{i\geq 1}$ such that

$$n=\begin{cases}1 & \text{if } 0<\gamma<\gamma_1,\\ i+1 & \text{if } \gamma_i<\gamma<\gamma_{i+1},\end{cases}$$

and thus these are exactly the values of γ at which P_0 is discontinuous.

The dependence on the aspect ratio of any bifurcated steady state, as given by (6.2), has a clear interpretation in the framework of dynamic transitions. Namely, using γ as a control parameter and a bifurcated solution as a basic steady state, the system (3.1) undergoes a catastrophic transition at each γ_i. An important feature of such a transition is that, as γ crosses each γ_i, the number of rolls in the fluid changes from $2i$ to $2i+2$. For example, for $N=N_2$, the bifurcated steady state solution corresponding to $\gamma=3<\gamma_1$ has a two-roll pattern, as shown in Figure 6.2, and for $\gamma_1<\gamma=5<\gamma_2$, it has a four-roll pattern, as shown in Figure 6.3.

From Figure 6.1 we can also extract a rough transition diagram. More precisely, we note that at γ_1 (the first discontinuity point of P), the left limit is negative infinity, whereas the right limit is a finite negative number; similarly, at γ_i, $i>1$, the left and right limits are both finite negative numbers, with the left limit being greater than the right one. Accordingly, we see that any bifurcated solution $\mathbf{U}_s$ (see (6.2)), satisfies

$$\lim_{\gamma\to\gamma_1^-}\mathbf{U}_s(\gamma)=\mathbf{0},\qquad \lim_{\gamma\to\gamma_1^+}\mathbf{U}_s(\gamma)=\mathbf{U}_s(\gamma_1),$$

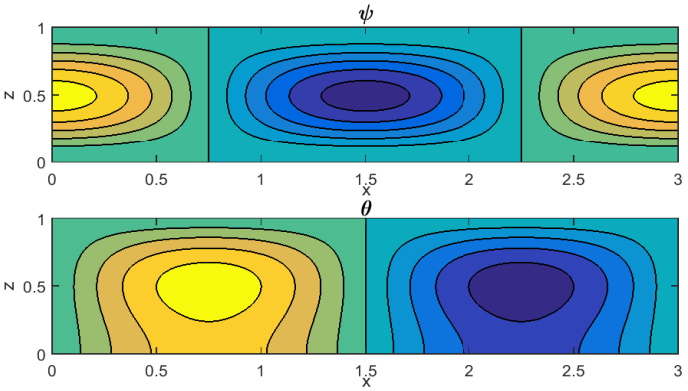

Fig. 6.2: *Bifurcated solution with a two-roll pattern for* $\gamma = 3$ $(\gamma < \gamma_1)$, $N = N_2$ *and* $n = 1$

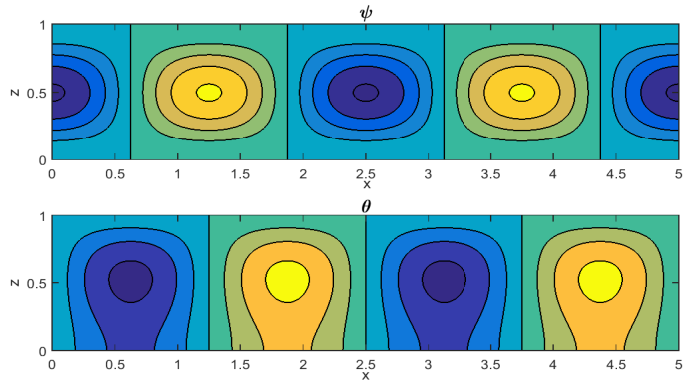

Fig. 6.3: *Bifurcated solution with a four-roll pattern for* $\gamma = 5$ $(\in (\gamma_1, \gamma_2))$, $N = N_2$ *and* $n = 2$

and, for $i > 1$,

$$\lim_{\gamma \to \gamma_i^-} \mathbf{U}_s(\gamma) = \mathbf{U}_s(\gamma_i^-), \qquad \lim_{\gamma \to \gamma_i^+} \mathbf{U}_s(\gamma) = \mathbf{U}_s(\gamma_i^+),$$

with

$$|\mathbf{U}_s(\gamma_i^-)| > |\mathbf{U}_s(\gamma_i^+)|.$$

Figures 6.5a and 6.5b show the bifurcation diagrams corresponding to these two situations.

Finally, we note that, as can be seen from (7.3), the transition number P_0 in the absence of heating sources and with constant gravity, is asymptotically proportional to the Prandtl number Pr when Pr is large, which is the regime under consideration. This property is retained by the general case of non-zero heating source and varying gravity. To see this, we compute as before the values of the transition number for Pr in the range $[10, 100]$. The aforementioned scaling property is then clear from Figure 6.4. Note also that when the magnitude of the transition number P increases, the size of the basic solution (2.4) decreases. Since Pr is proportional to kinematic viscosity ν, which from a physical perspective is inversely proportional to the typical velocity of the fluid

particles, we see that the fact that transition number P is asymptotically proportional to the Prandtl number is consistent with physical reality.

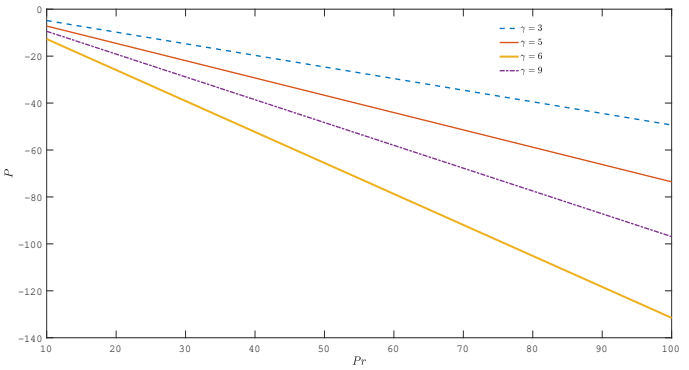

Fig. 6.4: *The transition number P given in (5.16) for $N = N_2$ and different values of γ, with respect to the Prandtl number.*

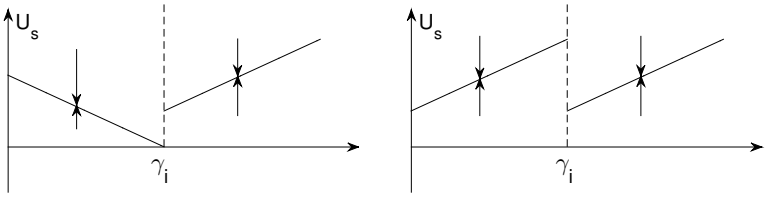

(a) $i = 1$ (b) $i > 1$

Fig. 6.5: *Bifurcation diagrams of the second transition relative to the zero solution*

Appendix. In this section we derive an explicit formula for the transition number corresponding to (3.1), subject to the boundary conditions

$$\begin{aligned} &\psi(x+\gamma,z) = \psi(x,z), \\ &\psi(x,0) = \psi(x,1) = \frac{\partial^2\psi}{\partial z^2}(x,0) = \frac{\partial^2\psi}{\partial z^2}(x,1) = 0, \end{aligned} \tag{7.1}$$

$$\theta(x+\gamma,z) = \theta(x,z), \qquad \theta(x,1) = \theta(x,0) = 0. \tag{7.2}$$

We assume also that H and N are given positive constants. Then, setting $\beta = 0$, the critical mode e_m can be found explicitly as

$$e_n = e^{ia_n x} \begin{pmatrix} \alpha\sqrt{\frac{H}{N}}\sin\pi z \\ -i\sqrt{\pi^2 + a_n^2}\,\alpha\sin\pi z \end{pmatrix}$$

where $\alpha \in \mathbb{C}$ is an arbitrary normalization constant.

The solution e_n^* of the dual problem,

$$\overline{\beta}\mathcal{A}_n^* u = \mathcal{L}_n^* u$$

where

$$\mathcal{L}_n^*(\Psi,\Theta) = \begin{pmatrix} (\partial_z^2 - a_n^2)^2\Psi + ia_n RN(z)\Theta \\ (\partial_z^2 - a_n^2)\Theta + ia_n RH(z)\Psi \end{pmatrix}$$

and the boundary conditions are the same as above, can also be found explicitly and is given by

$$e_n^* = e^{ia_n x}\begin{pmatrix} \alpha^*\sqrt{\frac{N}{H}}\sin\pi z \\ i\sqrt{\pi^2+a_n^2}\alpha^*\sin\pi z \end{pmatrix}.$$

Note that we have the property

$$\langle \mathcal{A}_n e_n, e_n^*\rangle = -\alpha\overline{\alpha^*}\gamma(\pi^2+a_n^2)\frac{1+Pr}{2}.$$

Regarding the nonlinear interactions, we have that

$$\mathcal{G}(e_n,e_n) = \mathcal{G}(e_{-n},e_{-n}) = 0,$$

$$\mathcal{G}(e_n,e_{-n}) = ia_n\begin{pmatrix} -\frac{H}{N}2\pi|\alpha|^2(\pi^2+a_n^2)\sin\pi z\cos\pi z \\ i\sqrt{\frac{H}{N}}2\pi|\alpha|^2\sqrt{\pi^2+a_n^2}\mathrm{Pr}\sin\pi z\cos\pi z \end{pmatrix}$$

$$\mathcal{G}(e_{-n},e_n) = -ia_n\begin{pmatrix} -\frac{H}{N}2\pi|\alpha|^2(\pi^2+a_n^2)\sin\pi z\cos\pi z \\ -i\sqrt{\frac{H}{N}}2\pi|\alpha|^2\sqrt{\pi^2+a_n^2}\mathrm{Pr}\sin\pi z\cos\pi z \end{pmatrix}$$

By using the same procedure outlined in Section 5, we find that

$$\partial_z\Theta_{11}(z) = i\sqrt{\frac{H}{N}}|\alpha|^2\sqrt{\pi^2+a_n^2}\mathrm{Pr}\cos 2\pi z, \quad \Psi_{11}\equiv 0$$

and

$$\mathcal{G}(\Phi_{11},e_n) = 0,$$

$$\mathcal{G}(e_n,\Phi_{11}) = e^{ia_n x}\begin{pmatrix} 0 \\ -i\frac{H}{N}\mathrm{Pr}^2\sqrt{\pi^2+a_n^2}a_n^2|\alpha|^2\alpha\sin\pi z\cos 2\pi z \end{pmatrix}$$

so that

$$\langle \mathcal{G}(e_n,\Phi_{11}) + \mathcal{G}(\Phi_{11},e_n), e_n^*\rangle = \frac{\mathrm{Pr}^2 H}{4N}\gamma(\pi^2+a_n^2)a_n^2|\alpha|^2\alpha\overline{\alpha^*}$$

Then, assuming that the first eigenfunction e_m is normalized under the inner product

$$(u,v) = \frac{1}{\gamma}\int_0^\gamma\int_0^1 u\overline{v}dxdz,$$

we obtain

$$|\alpha|^2 = \frac{2}{(\frac{H}{N} + \pi^2 + a_n^2)},$$

from where the transition number P_0 is found to be

$$P_0 = -\frac{H\mathrm{Pr}^2 a_n^2}{(1+\mathrm{Pr})(H + N\pi^2 + Na_n^2)}. \tag{7.3}$$

REFERENCES

[1] F. H. Busse, *Transition to turbulence in Rayleigh-Bénard convection*, in: H. L. Swinney and J. P. Gollub (Eds.) Hydrodynamic Instabilities and the Transition to Turbulence, Topics Appl. Phys., Springer, Berlin, 45:97–137, 1985. 1

[2] S. Chandrasekhar, *Hydrodynamic and Hydromagnetic Stability*, Courier Corporation, 1962. 1

[3] H. Jeffreys, *The stability of a layer of fluid heated below*, Philos. Mag. (7), 2(10):833–844, 1926. 1

[4] V. Iudovich, *Free convection and bifurcation*, J. Appl. Math. Mech., 31(1):103–114, 1967. 1

[5] A. Pellew and R. V. Southwell, *On maintained convective motion in a fluid heated from below*, Proc. R. Soc. Lond. A Math. Phys. Sci., 176:312–343, 1940. 1

[6] K. Kirchgässner, *Bifurcation in nonlinear hydrodynamic stability*, SIAM Rev., 17(4):652–683, 1975. 1

[7] T. Ma and S. Wang, *Attractor bifurcation theory and its applications to Rayleigh-Bénard convection*, Commun. Pure Appl. Anal., 2(4):591–599, 2003. 1

[8] P. H. Rabinowitz, *Existence and nonuniqueness of rectangular solutions of the Bénard problem*, Arch. Ration. Mech. Anal., 29:32–57, 1968. 1

[9] T. Ma and S. Wang, *Dynamic bifurcation and stability in the Rayleigh-Bénard convection*, Commun. Math. Sci., 2(2):159–183, 2004. 1

[10] C.-H. Hsia, T. Ma, and S. Wang, *Stratified rotating Boussinesq equations in geophysical fluid dynamics: dynamic bifurcation and periodic solutions*, J. Math. Phys., 48(06):065602, 2007. 1

[11] C.-H. Hsia, T. Ma, and S. Wang, *Rotating Boussinesq equations: dynamic stability and transitions*, Discrete Contin. Dyn. Syst., 28(1):99–130, 2010. 1

[12] C.-H. Hsia, C.-S. Lin, T. Ma, and S. Wang, *Tropical atmospheric circulations with humidity effects*, Proc. R. Soc. A., 471(2173):20140353, 24, 2015. 1

[13] G. K. Pradhan and P. C. Samal, *Thermal stability of a fluid layer under variable body forces*, J. Math. Anal. Appl., 122(2):487–495, 1987. 1

[14] B. Straughan, *The Energy Method, Stability, and Nonlinear Convection*, Second Edition, Appl. Math. Sci., Springer-Verlag, New York, 91, 2004. 1, 2, 6

[15] I. H. Herron, *On the principle of exchange of stabilities in Rayleigh-Bénard convection*, SIAM J. Appl. Math., 61(4):1362–1368, 2001. 1, 4

[16] I. H. Herron, *On the principle of exchange of stabilities in Rayleigh-Bénard convection II. No-slip boundary conditions*, Ann. Univ. Ferrara Sez. VII (N.S.), 49:169–182, 2003. 1, 4

[17] T. Ma and S. Wang, *Phase Transition Dynamics*, Springer, New York, 2014. 1, 3, 5, 5, 5

[18] J. Shen, T. Tang, and L.-L. Wang, *Spectral Methods: Algorithms, Analysis and Applications*, Springer Science & Business Media, 41, 2011. 4, 6